Taming Self-Organization Dynamics to Dramatically Control Porous Architectures

Ronan Daly, [*†,∥] *John E. Sader,* [‡,§] *John J. Boland* [†]

[†] School of Chemistry and Centre for Research on Adaptive Nanostructures and Nanodevices (CRANN), University of Dublin, Trinity College Dublin, Dublin 2, Ireland.

[‡] School of Mathematics and Statistics, The University of Melbourne, Victoria 3010, Australia.

[§] School of Physics and Centre for Research on Adaptive Nanostructures and Nanodevices (CRANN), University of Dublin, Trinity College Dublin, Dublin 2, Ireland.

KEYWORDS: Self-organization, breath figures, non-coalescence, water droplet, soft lithography, honeycomb.

ABSTRACT: We demonstrate templating of functional materials with unexpected and intricate micro and nanostructures by controlling the condensation, packing and evaporation of water droplets on a polymer solution. Spontaneous evaporation of a polymer solution induces cooling of the liquid surface and water microdroplet condensation from the ambient vapor. These droplets pack together and act as a template to imprint an entangled polymer film. This Breath Figure (BF)

phenomenon is an example of self-organization that involves the long-range ordering of droplets. Equilibrium-based analysis provides many insights into contact angles and drop stability of individual drops but the BF phenomenon remains poorly understood thus so far preventing translation to real applications. Here we investigate the dynamics of this phenomenon to separate out the competing influences and then introduce a modulation scheme to ultimately manipulate the water vapor-liquid-equilibrium independently from the solvent evaporation. This approach to BF control provides insights into the mechanism, a rationale for microstructure design and evidence for the benefits of dynamical control of self-organisation systems. We finally present dramatically different porous architectures from this approach reminiscent of microscale Petri-dishes, conical flasks and test-tubes.

In 1911 Lord Rayleigh examined closely the condensation and evaporation of patterns of water droplets on a glass plate, noting especially the droplet edge pinning and changes in contact angle[1]. Known as breath figures (BFs), this has more recently become the subject of intense research with the focus still on the three-phase interface behavior.The current growth in interest can be traced back to the pioneering work observing and controlling breath figures on liquid surfaces[2 - 5]. Francois *et al*.[6] and Limaya *et al*.[7] noted that the same condensation phenomenon can be applied to polymer solutions when using volatile solvents to give ordered, non-coalescing arrays of droplets. The use of volatile solvents was explored because the droplets actually served to imprint their shape into the final polymeric film, thus providing a facile and inexpensive route

to form a porous polymeric microstructure[8, 9] and explain the earlier observations by Widawski *et al.*[10]

Numerous studies have sought to control pore size and pore mono-dispersity by understanding the non-coalescence phenomenon of the templating microdroplets[11-16] while others have used the same approach to template hierarchical assemblies of nanoparticles or other functional molecules for specific applications[17-23] *e.g.* controlled drug release. The vast majority of reported microstructures are comprised of close-packed pores whose spherical shapes reflect that of the imprinted water droplets, while any reasons for minor deviations have not been explored or explained.

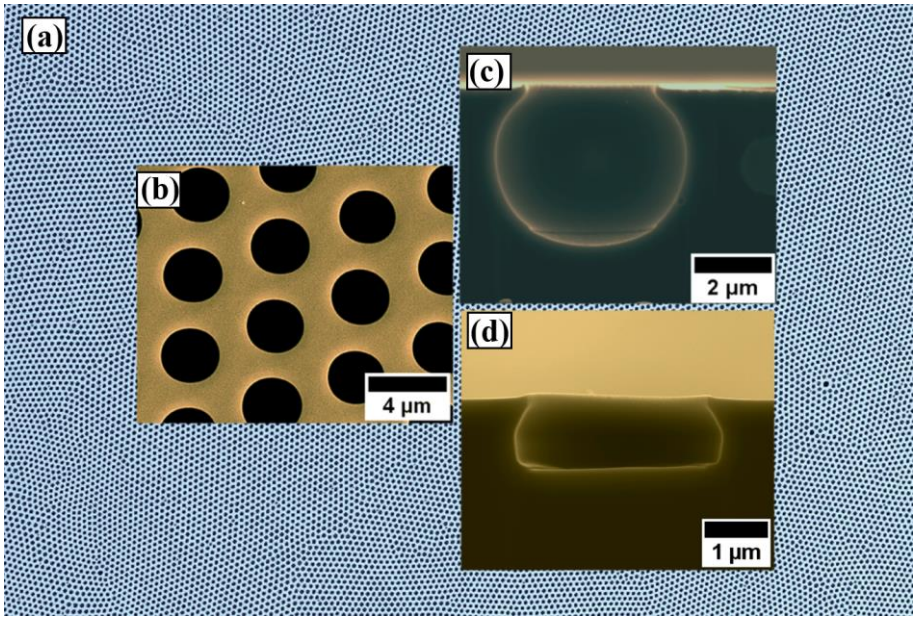

Figure 1. Electron microscopy images of (a) an ordered microporous polystyrene film with clear domain boundaries, (b)-(c) high magnification plan and cross-sectional views of a microporous polystyrene film with spherical pores, (d) a high-angle view of a shallow-pore architecture.

Figure 1(a) shows a scanning electron microscopy (SEM) micrograph of ordered pore patterns formed by this technique in a dicarboxy-terminated polystyrene (DCPS) film, while Figures 1(b)-(c) show higher magnification images and a cross-section of the film that reveals the spherical nature of the assembled pores. The fidelity of this imprinting phenomenon, as seen in Figure 1(c), is evidently due to maintaining conditions where the surface tension of the water droplet is the dominant factor in controlling shape and this is ultimately transferred to the pore microstructure. Here, we demonstrate that the shapes do not have to be controlled by surface tension alone and the microstructure can be manipulated by controlling the timing of the water phase change events and the local polymer composition. In particular, we introduce an easy-to-implement modulated growth scheme that separately controls the preparation of the polymer surface and the delivery of water droplets onto that surface. This provides insights into the system dynamics, and in addition the ability to create arrays of previous unknown porous microstructures that range in shape from microscale Petri-dishes (Figure 1d), conical flasks and round bottom flasks to test-tube like structures (shown later in Figure 4a-f).

RESULTS AND DISCUSSION

Dynamic System. Traditionally, experiments are performed under static or slow continuous air flow conditions. This approach is straight forward to set up and can provide a repeatable, well controlled environment. Water-entrained gas (nitrogen, argon or air) is maintained at a fixed, specified relative humidity (RH) and passed over a polymer solution containing a volatile solvent. Solvent evaporation causes surface cooling and when the temperature drops below the dew point corresponding to these RH conditions, condensation of water drops can occur. While

the latent heat of vaporization of the solvent is the major factor determining the achievable temperature drop, the presence of polymer and elevated humidity conditions modifies the thermal path of the evaporating sample. An example supporting this is shown in the Supporting Information (S.I. 1) and illustrates the thermal path for two different solvents evaporating at six different values of relative humidity. The condensed droplets then grow in size [3, 24, 25] and self-organize into close-packed arrays to create a template that is transferred into the polymer. It has been proposed that the drops do not coalesce during this process due to a combination of polymer precipitation at the drop interfaces and the presence of a thin layer of solvent [26]. As this process continues, the polymer concentration increases, evaporation slows and the temperature of the solution begins to rise again, returning above the dew point. At this point, the water vapor-liquid-equilibrium (VLE) switches direction and the droplets begin to evaporate. In the standard approaches reported, this VLE switch always happens after a sufficient increase in polymer concentration for the droplets to template the film permanently, with resulting pores retaining the spherical droplet shape. To explore the dynamics of this system more fully, we modify the timing of this switch by controlling solvent evaporation and relative humidity independently. This is achieved by separately modulating the gas flow rate and relative humidity over the polymer solution and provides unprecedented control of key process parameters: temperature, relative humidity, air flow rates and mass gain/loss. In addition to unique insights into the breath figure phenomenon this approach facilitates a dramatic level of microstructure control.

Microstructure Control. The first step in controlling the final microstructure lies in identifying the critical onset conditions where pores are first formed under a continuous vapor flow. The onset is clearly observable even without a microscope because an area of closely packed pores in

a polymer film appears white or iridescent due to the scattering of light. By creating a set of samples, each formed using a targeted, constant air flow rate at a controlled RH, we found that the onset humidity is constant for a given solvent/polymer solution. The critical onset humidities, for a chloroform/DCPS solution, over a range of gas flow rates are shown in Figure 2(a). Error bars in the x-axis reflect the graduated scale of the flow meter, while the errors in the y-axis represent the experimental step size between no pore observation and pore onset. Solvent evaporation and hence cooling occurs more rapidly at faster air flow rates or with solvents of a higher vapor pressure. This claim is quantitatively measured and reported in S.I. 3 and S.I. 4. By lowering the achievable temperature, this technique drives an associated lowering of the critical onset humidity. The critical onset humidity was examined for three solvents under identical conditions and it is shown in S.I. 5 that the onset value increases linearly with solvent boiling point. This confirms firstly that the critical onset humidity is simply due to the ease with which a solvent can leave the bulk (*i.e.* latent heat of vaporization), thus driving evaporative cooling and secondly, that this is a predictable value, as evidenced by the data in S.I. 5. These critical onset humidities, reported here for the first time, dictate which solvents are effective at pore formation under particular flow rates and RH conditions.

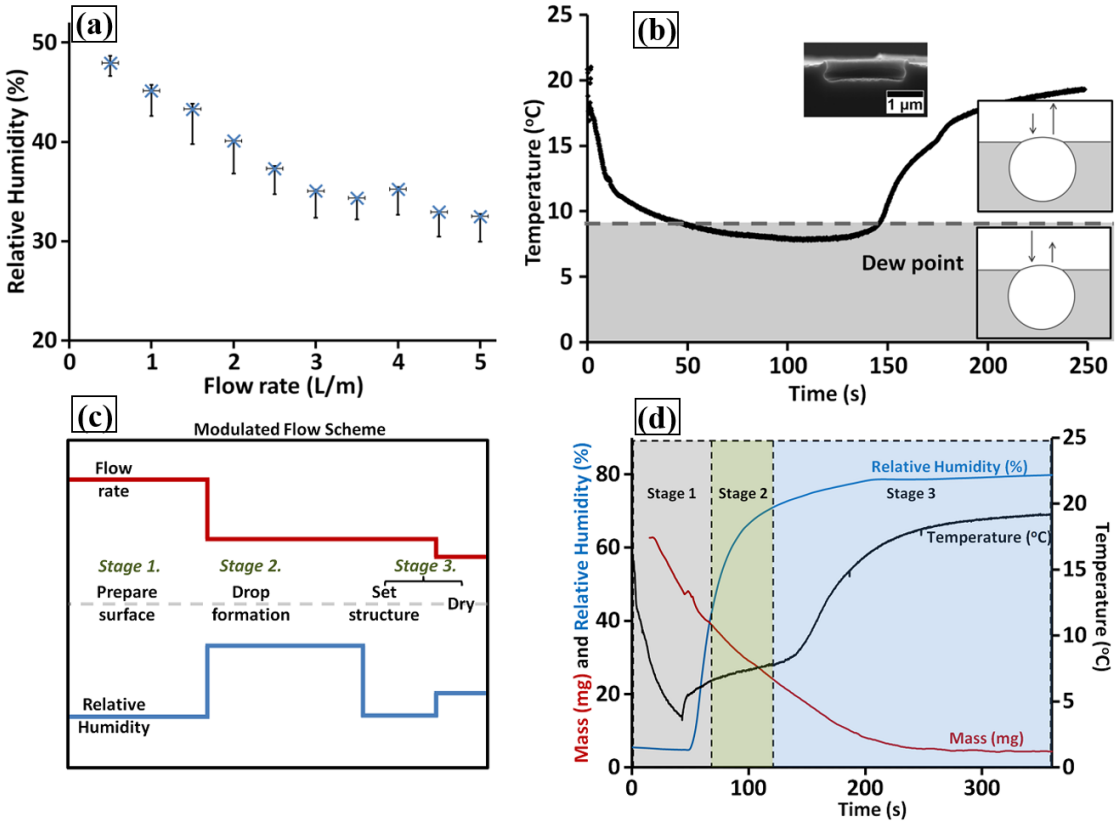

Figure 2. (a) Change in critical onset humidity with flow rate for chloroform-DCPS solution.(b) Temperature profile for 3.5%$_{w/w}$ chloroform-DCPS solution evaporating with air flow at 1L/min. The inset image shows a pore formed under these conditions. (c) Modulation strategy for sample preparation in 3 stages. (d) Combined mass, temperature and humidity measurement with the 3 stages indicated. Stage 1 is carried out at 5L min^{-1}, sections 2-3 at 1 L min^{-1}.

A robust set of experiments examined the achievable pore opening dimensions (rather than pore volume) attainable from a set of three solvents. A remarkable cross-solvent trend (shown in S.I. 6) is observed for achievable pore size and can be used in conjunction with this critical humidity data to provide control over both pore formation and pore size.

Focusing on chloroform/DCPS solutions, the dynamics of the system can be understood through closer examination of the solution temperature path at a 1 L/min flow of vapor, as shown in Figure 2(b). This corresponds to the critical onset humidity of 45% noted in Figure 2a. The characteristic temperature path for the constant flow experiment shows an initial drop in temperature due to evaporative cooling of the solvent causing droplet condensation. As the polymer concentration rises, evaporative cooling is reduced and heat is absorbed from the surroundings. The water droplet dew-point of 9^{o}C illustrated in Figure 2(b) is consistent with that predicted by Antoine's equation. This represents the temperature where the rate of water condensation is balanced by the rate of evaporation and shows that droplet formation and templating is expected to occur over a very limited time interval. Clearly, with an independent means to control the surface temperature and/or the ambient RH, it is possible to manipulate the VLE to control this condensation/evaporation phenomenon and the duration of time available for each. The Supporting Information contains a video that demonstrates this VLE control, where high magnification optical microscopy of the growth and packing of droplets and their subsequent shrinkage as the VLE is switched by controlling the RH of the ambient vapor.

Under the critical onset conditions shown in Figure 2(b), and despite the short time duration available for condensation, the droplets are still able to imprint their shapes onto the polymer. Remarkably, however, the imprinted pore shape bears little resemblance to a spherical droplet. Across the entire range of onset conditions shown in Figure 2(a), the imprinted pores all have the same structure; they are flat-based and shallow pores, with shapes that are reminiscent of Petri dishes (see inset Figure 2b). The fact that this new morphology is highly ordered and mono-disperse (see inset Figure 1a) indicates that it originates from the same non-coalescing breath

figure phenomenon and this is directly confirmed by optical microscopy. Pores formed at RH levels above the continuous flow onset conditions in Figure 2(a) invariably have a spherical shape until very high humidities lead to pore destabilization and coalescence. Based on these observations, it is speculated that the ability to create non-spherical pores depends on controlling the polymer solution properties independently from the phase change behavior of the water. To tune the solution surface, we developed a system to actively and independently modulate the gas/vapor flow rate, composition and flow duration. The modulated growth scheme is comprised of three stages, namely:

Stage I: A polymer solution surface preparation stage; introducing a fast, dry flow that drops the surface temperature without introducing water condensation,

Stage II: A controlled droplet condensation stage at a targeted flow rate and RH, and finally

Stage III: A sample drying stage of known flow rates and RH leading to the final polymer film. The conditions during this stage determine whether water droplets or the organic solvent evaporates first.

This approach provides access to a dramatically wider range of porous microstructures than previously possible. Figure 3 summarizes the range of pore morphologies found so far using our modulated flow technique (in blue outlined boxes), in contrast to that provided by the conventional continuous flow method (red outlined boxes). To help visualize the entire phase space in a 2D representation, the horizontal axis is the total exposure of the solution surface to air expressed in units of liters (L), achieved by combining the flow rate profile (L min^{-1}) and the time of exposure (min).

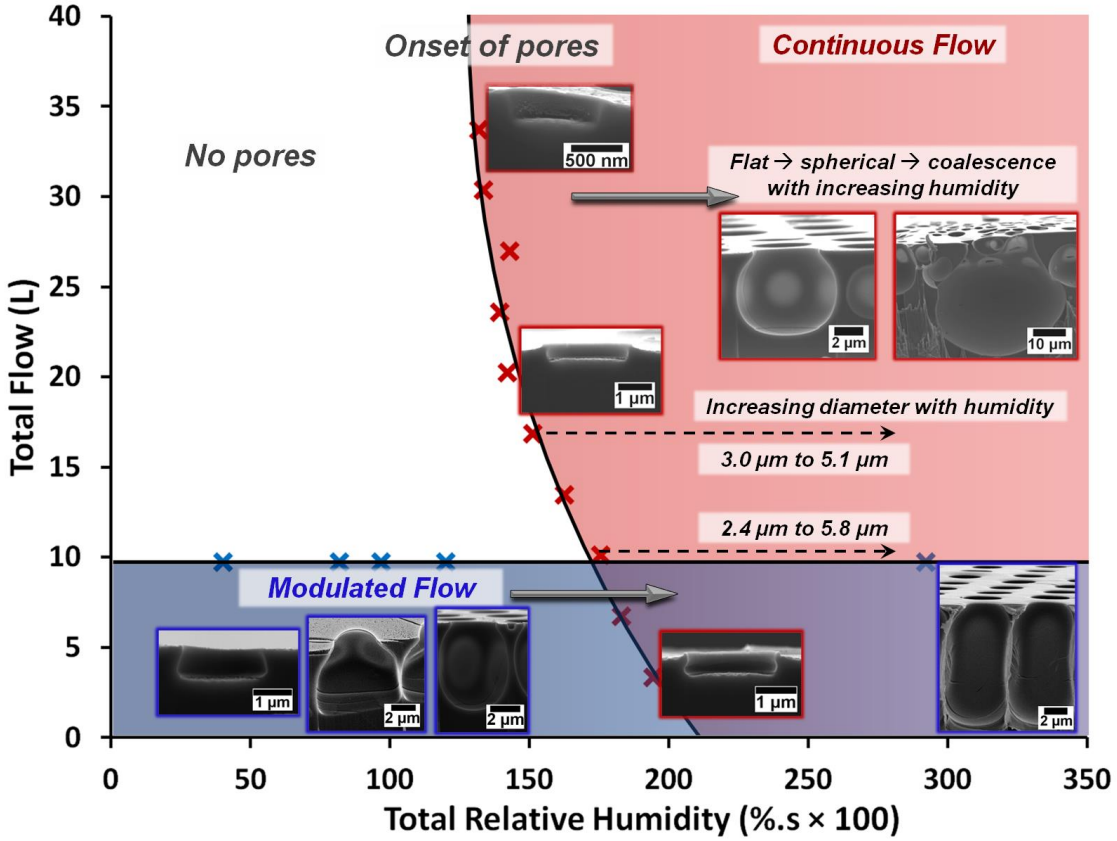

Figure 3: Phase space for BF templating with a 3.5%$_{w/w}$ chloroform/DCPS solution. In red, the constant flow method has a critical onset humidity boundary. A separate phase space (blue) can be accessed with modulated flow and alternative pore shapes can be fabricated.

Similarly, the vertical axis is the total integrated RH exposure for the time of exposure (%RH. s), which is dominated by Stage II and III conditions since 0% RH air is used in Stage 1. The details of flow-rates, %RH and time durations for Stage I-III for the points marked in Figure 3 are presented in full in S.I. 7. As expected, the continuous flow approach exhibits an immediate boundary associated with the pore onset condition (curve defined by red × in Figure 3), described in Figure 2(a). Along this boundary, flat-based, shallow pores are always obtained, as described earlier. At higher RH values, spherical pores are observed as reported in the literature. Moving

further along the x-axis under these continuous flow conditions, larger pore sizes are observed and eventually pore coalescence and reduced monodispersity are also recorded.

The modulation scheme provides for the separate preparation of the surface conditions during Stage 1 prior to condensation and pore growth in Stage 2. It is this ability to prepare the surface of the polymer solution in Stage I without driving condensation that provides access to porous microstructures in a previously inaccessible region of phase space. Clearly many combinations of conditions are possible across the three stages. The data in Figure 3 corresponds to a fixed Stage 1 condition of 45 seconds in duration at 5 L/min flow rate and 0% RH. By maintaining this condition and varying Stage II and III within a fixed overall experimental time, results in the progression of porous microstructures of increasing depths, as shown in Figure 3 in the blue shaded regions. At the shortest RH exposures in Stage II, we observed very shallow Petri-dish shaped micropores, similar to the onset pore geometry found under continuous flow conditions. Continuing to increase exposure to RH leads to standard spherical pores and then remarkably to a previously inaccessible region of phase space with cylindrical pores. These structures are very interesting because of the difficulty in making high aspect ratio features with nanoscale wall thicknesses (approximately 30nm, measured using a helium ion microscope).

The portion of the experimental phase space explored in Figure 3 captures the accessible pore structures starting from just a single set of conditions and for a given initial polymer concentration and solvent. Clearly the number of possible conditions (and hence morphologies) is very large. For example, when examining other solvent systems, it was noted that toluene led to a single layer of pores, similar to those reported for chloroform. However, dichloromethane led to a foam-like multi-layer structure as shown in Figure 4(a). Using the modulation technique,

this multi-layer structure was consistently reduced to a single layer of pores, as shown in Figure 4(b). The details of the experimental conditions are provided in S.I.8.

The modulation system is observed to uniquely allow control over pore shape without compromising the ordering process. In all of the cases examined, we have maintained the same initial drying step (Stage 1) and so water droplets must begin to condense, grow and order in very similar conditions for all of the modulation techniques applied. However, it is the presence of the consistently high humidity that leads to long, cylindrical pores and the sudden low humidity that leads to shallow, Petri-dish pores. The ordering for these structures can be seen in Figure 4 (c-d). An example of the shallowest features observed is shown in Figure 4(e), with all detailed experimental timings available in S.I. 7.

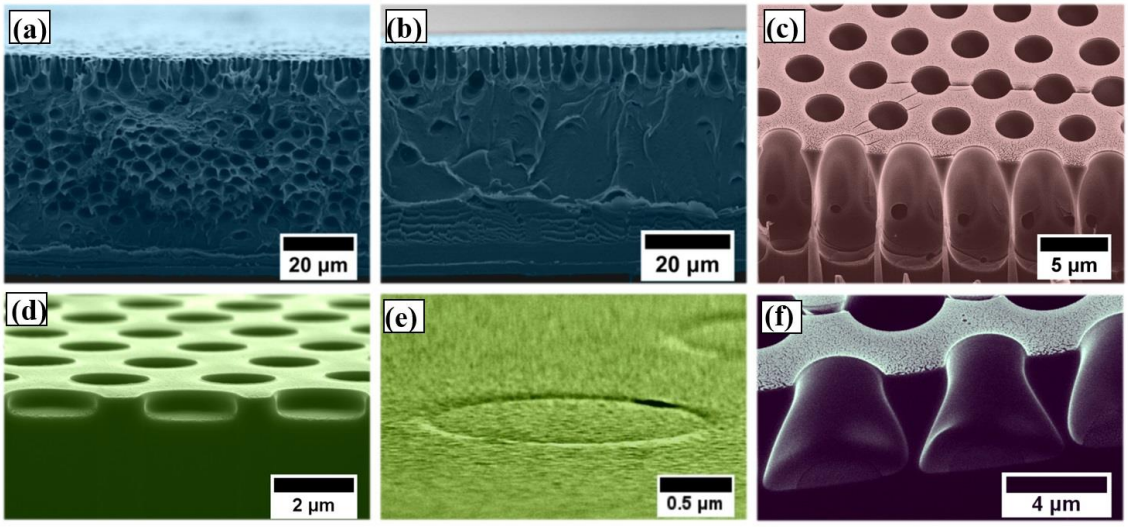

Figure 4: (a) 70% RH continuous flow with DCM/DCPS solution, (b) modulated flow 5% to 70% RH with DCM/DCPS solution, (c) modulated flow from <5% to 85% RH with chloroform/DCPS to give elongated pores, (d)-(e) almost full recovery of surface leading to arrays of shallow pores and imprints, (f) conical-flask pores formed at 5% $_{w/w}$ DCPS in chloroform. Full details of experimental conditions are given in S.I. 7.

While mapping the complete range of possible parameters is not the focus of this manuscript, some additional findings should be noted. As expected, with an increase in polymer concentration and a subsequent drop in the rate of solvent evaporation, the final drop size and pore opening size decreases. For constant flow experiments this ranged from 4-5 μm pore opening diameters at 3% $_{w/w}$ to 2.6 μm at 5% $_{w/w}$. Once the polymer concentration reaches too high a level (*e.g.* 8% $_{w/w}$), the system becomes poorly controllable with a wide pore size distribution and polymer skin formation reducing the rate of evaporation further. The microstructure also changes from standard spherical pores (Figure 1c) at 3-4% $_{w/w}$ to conical flask shapes at 7-8% $_{w/w}$ as shown in Figure 4(f).

The observations from the detailed phase-space mapping carried out so far allow us to speculate on the underlying pore formation mechanism. The observation of flat-base pores for instance suggests that by switching the VLE of the water droplets, the droplets evaporate prior to the surrounding polymer becoming fully set. The upper surface is always the first to set, due to the solvent-evaporation-driven concentration gradient. Without the droplet to maintain the pore integrity, the viscous polymer solution can begin to recover, flattening the base of the pores. If a surface is allowed to continue to recover until the pores have completely vanished, there are often ordered arrays of features on the surface, such as very shallow imprints as seen in Figure 4(d-e). The chosen modulated approach drives a rapid evaporation without inducing water condensation. This is believed to lead to a cold surface, a more viscous sample and also a concentration gradient of polymer. On the other hand elongated pore structures are formed because this concentration gradient propagates downwards during evaporation and stabilizes the upper part of the drop, preventing a Rayleigh instability, while still allowing droplet growth into the lower section. This can only occur under very particular conditions. A wide range of volatile solvents have been

explored in the literature, most commonly carbon disulphide[9, 10, 27], toluene, chloroform[28, 29], and THF[28, 30, 31]. We note that the droplets can be highly unstable at the interface and with a very volatile solventsuch as dichloromethane. The droplets can be swept below the surface on convection currents[32], leading to a similar process to emulsion templating. This can again be switched off by a modulation approach, which will increase the solution viscosity due to both a drop in temperature and increase in polymer concentration, cutting off the strong currents[33].

CONCLUSIONS

The results of previous work indicated that the solvent determines the droplet positioning at the solution/air interfac[29, 34]. Here, by considering the dew point temperature, a solvent can be linked to both the flow rate required and the final pore size expected under constant flow conditions (S.I. 6). It is clearly shown that a much greater range of pore geometries are accessible than previously noted with a modulated flow technique. By exploiting the dynamical nature of BF templating, a heuristic has been developed to imprint into a polymer solution of controlled polymer concentration gradient and subsequently, to control relaxation flow and to "dial-in" a broad spectrum of microstructures. Current work is focusing on the expanding to other self-organization systems, conformal coating and functional particulate applications, with early examples shown in S.I. 9. In addition modelling of the concentration gradient dynamics and stabilization mechanism is planned to help elucidate further the feasible controls and to allow commercial applications to develop at a more rapid pace.

METHODS

The solvents used to examine breath figure templating were (i) chloroform for spectroscopy, Uvasol® supplied by Merck, (ii) toluene puriss., absolute, over molecular sieve ($H_2O \leq 0.005\%$), $\geq 99.7\%$ (GC) supplied by Sigma Aldrich and (iii) dichloromethane, HPLC grade. Water was both de-ionized and filtered. The polymer used was α, ω Dicarboxy terminated Polystyrene (DCPS), $Mn = 93.8 \times 10^3$, $Mw/Mn = 1.07$, Polymer Source. The detailed experimental arrangement is reported in previous work[29] and a diagram is presented in the Supporting Information (S.I. 2). The flow of carrier gas (99.999% nitrogen) is controlled by a flow controller/meter arrangement. The relative humidity (RH) is controlled by first passing part of this stream through a humidifier with a feedback control based on a hygrometer at the point of sample deposition. The growth chamber includes a port for dosing the polymer solution onto a glass cover slip. The mass and temperature changes during the formation process can be recorded by the in-situ mass balance and ultra-fine thermocouple incorporated into the chamber. The entire process can be monitored in real time by optical microscopy. This setup allows the rapid, independent modulation of the flow rate and relative humidity and the appropriate measurements to understand the solution's response.

ASSOCIATED CONTENT

Supporting Information. A brief statement in non-sentence format listing the contents of material supplied as Supporting Information should be included, ending with "This material is available free of charge *via* the Internet at http://pubs.acs.org." For instructions on what should be included in the Supporting Information, as well as how to prepare this material for publication, refer to the journal's Instructions for Authors.

This material is available free of charge *via* the ACS Publications website at http://pubs.acs.org.

AUTHOR INFORMATION

Corresponding Author

* E-mail: rd439@cam.ac.uk, Tel.: +44 (0)1223 766065

Present Address

‖ Department of Engineering, University of Cambridge, 17 Charles Babbage Road, Cambridge CB3 0FS, United Kingdom.

Author Contributions

The manuscript was written through equal contributions from all authors. All authors have given approval to the final version of the manuscript.

Funding Sources

The financial support of Science Foundation Ireland (Grant No. 06/IN.1/I106) and the Australian Research Council grants scheme are gratefully acknowledged.

REFERENCES

1. Rayleigh, L. Breath Figures. *Nature* **1911**, *86*, 416–417.
2. Knobler, C. M.; Beysens D. Growth of Breath Figures on Fluid Surfaces. *Europhys. Lett.* **1988**, *6*, 707–712.
3. Steyer, A.; Guenoun P.; Beysens, D. Two-Dimensional Ordering During Droplet Growth on a Liquid Surface. *Phys. Rev. B* **1990**, *42*, 1086–1090.
4. Beysens, D.; Steyer, A.; Guenoun, P.; Fritter D., Knobler, C.M. How Does Dew Form? *Phase Transit.* **1991**, *31*, 219–246.

5. Steyer, A.; Guenoun, P.; Beysens, D. Hexatic and Fat-Fractal Structures for Water Droplets Condensing on Oil, *Phys. Rev. E* **1993**, *48*, 428–433.
6. Francois, B.; Pitois, O.; Francois J. Polymer Films with a Self-Organized Honeycomb Morphology, *Adv. Mater.* **1995**, *7*, 1041–1044.
7. Limaye, A. V.; Narhe, R. D.; Dhote, A. M.; Ogale, S. B. Evidence for Convective Effects in Breath Figure Formation on Volatile Fluid Surfaces, *Phys. Rev. Lett.* **1996**, *76*, 3762–3765.
8. Karthaus, O.; Maruyama, N.; Cieren, X.; Shimomura, M.; Hasegawa, H.; Hashimoto, T. Water-Assisted Formation of Micrometer-Size Honeycomb Patterns of Polymers, *Langmuir* **2000**, *16*, 6071–6076.
9. Srinivasarao, M.; Collings, D.; Philips A.; Patel, S. Three-Dimensionally Ordered Array of Air Bubbles in a Polymer Film. *Science* **2001**, *292*, 79–83.
10. Widawski, G.; Rawiso M.; François, B. Self-Organized Honeycomb Morphology of Star-Polymer Polystyrene Films. *Nature* **1994**, *369*, 387–389.
11. Bolognesi, A.; Mercogliano C.; Yunus, S. Self-Organization of Polystyrenes into Ordered Microstructured Films and Their Replication by Soft Lithography. *Langmuir* **2005**, *21*, 3480–3485.
12. Stenzel, M. H.; Barner-Kowollik, C.; Davis, T. P. Formation of Honeycomb-Structured, Porous Films *via* Breath Figures with Different Polymer Architectures. *J. Polym. Sci. Pol. Chem.* **2006**, *44*, 2363–2375.
13. Li, J.; Cheng, J.; Zhang, Y.; Gopalakrishnakone, P. Influence of Vacuum on the Formation of Porous Polymer Films *via* Water Droplets Templating. *Colloid Polym. Sci.* **2009**, *287*, 29–36.

14. Xu, Y.; Zhu B.; Xu, Y. A Study on Formation of Regular Honeycomb Pattern in Polysulfone Film. *Polymer* **2005**, *46*, 713–717.
15. Zhao, B. H.; Zhang, J.; Wu, H. Y.; Wang, X. D.; Li, C. X. Fabrication of Honeycomb Ordered Polycarbonate Films Using Water Droplets as Template. *Thin Solid Films* **2007**, *515*, 3629–3634.
16. Xiong, X.; Lin, M.; Zou, W.; Liu, X. Kinetic Control of Preparing Honeycomb Patterned Porous Film by the Method of Breath Figure. *React. Funct. Polym.* **2015**, *71*, 964–971.
17. Chari, K.; Lander C. W.; Sudol, R. J. Anamorphic Microlens Arrays Based on Breath-Figure Template with Adaptive Surface Reconstruction. *Appl. Phys. Lett.* **2008**, *92*, 111916.
18. Ma, C.-Y.; Zhong, Y-W.; Li, J.; Chen, K-C.; Gong, J-L.; Xie, S-Y.; Li, L.; Ma, Z. Patterned Carbon Nanotubes with Adjustable Array: A Functional Breath Figure Approach. *Chem. Mater.* **2010**, *22*, 2367–2374.
19. Munoz-Bonilla, A.; Ibarboure, E.; Papon E.; Rodriguez-Hernandez, J. Self-Organized Hierarchical Structures in Polymer Surfaces: Self-Assembled Nanostructures within Breath Figures. *Langmuir* **2009**, *25*, 6493–6499.
20. Xu, X.; Wang, X.; Nisar, A.; Liang, X.; Zhuang, J.; Hu, S.; Zhuang, Y. Combinatorial Hierarchically Ordered 2D Architectures Self-Assembled from Nanocrystal Building Blocks. *Adv. Mater.* **2008**, *20*, 3702–3708.
21. Yabu, H.; Hirai, Y.; Shimomura, M. Electroless Plating of Honeycomb and Pincushion Polymer Films Prepared by Self-Organization. *Langmuir* **2006**, *22*, 9760–9764.
22. Yabu, H.; Jia, R.; Matsuo, Y.; Ijiro, K.; Yamamoto, S-a.; Nishino, F.; Takaki, T.; Kuwahara, M.; Shimomura, M. Preparation of Highly Oriented Nano-Pit Arrays by

Thermal Shrinking of Honeycomb-Patterned Polymer Films. *Adv. Mater.* **2008**, *20*, 4200–4204.

23. De León, A.S.; Malhotra, S.; Molina, M.; Haag, R.; Calderón, M.; Rodríguez-Hernández J.; Muñoz-Bonilla, A. Dendritic Amphiphiles as Additives for Honeycomb-Like Patterned Surfaces by Breath Figures: Role of the Molecular Characteristics on the Pore Morphology, *J. Colloid Interf. Sci.* **2015**, *440*, 263–271.
24. Briscoe B.J.; Galvin, K.P. An Experimental Study of the Growth of Breath Figures. *Colloid Surface* **1991**, *56*, 263–278.
25. Beysens, D., Dew Nucleation and Growth. *C. R. Phys.* **2006**, *7*, 1082–1100.
26. Pitois O.; Francois, B. Formation of Ordered Micro-Porous Membranes. *Eur. Phys. J. B.* **1999**, *8*, 225–231.
27. Karthaus, O.; Cieren, X.; Maruyama, N.; Shimomura, M. Mesoscopic 2-D Ordering of Inorganicrorganic Hybrid Materials *Mat. Sci. Eng. C-Biomim.* **1999**, *10*, 103–106.
28. Peng, J.; Han, Y.; Yang, Y.; Li, B. The Influencing Factors on the Macroporous Formation in Polymer Films by Water Droplet Templating *Polymer* **2004**, *45*, 447–452.
29. Daly, R.; Sader J.E.; Boland, J.J. The Dominant Role of the Solvent/Water Interface in Water Droplet Templating of Polymers. *Soft Matter* **2013**, *9*, 7960–7965.
30. Park, M. S.; Kim, J. K. Breath Figure Patterns Prepared by Spin Coating in a Dry Environment. *Langmuir* **2004**, *20*, 5347–5352.
31. Cui, L.; Peng, J.; Ding, Y.; Li, X.; Han, Y. Ordered Porous Polymer Films *via* Phase Separation in Humidity Environment. *Polymer* **2005**, *46*, 5334–5340.

32. Maruyama, N.; Koito, T.; Nishida, J.; Sawadaishi, T.; Cieren, X.; Ijiro, K.; Karthaus, O.; Shimomura, M. Mesoscopic Patterns of Molecular Aggregates on Solid Substrates. *Thin Solid Films* **1998**, *327 – 329*, 854–856.
33. Koschmieder, E. L. *Bénard cells and Taylor vortices*, Cambridge University Press, 1993, pp. 11–53.
34. Daly, R.; Sader J. E.; Boland, J. J. Existence of Micrometer-Scale Water Droplets at Solvent/Air Interfaces. *Langmuir* **2012**, *28*, 13218–13223.